Ultrastructural and Morphological Observations of the External and Internal Structures of the Adult Midge *Culicoides grisescens* Edwards (Diptera: Ceratopogonidae)

Xue Lu , Yu Ling Zhang , Shun Cai Bao , Zhuang Fei Wang , Jing Ma , Nan Ling Zhou , Xiao Hui Hou *

Posted Date: 27 May 2024

doi: 10.20944/preprints202405.1715.v1

Keywords: Biting midge; Culicoides; morphology; scanning electron microscope; tissue sectioning

Article

Ultrastructural and Morphological Observations of the External and Internal Structures of the Adult Midge *Culicoides grisescens* Edwards (Diptera: Ceratopogonidae)

Xue Lu, Yu Ling Zhang, Shun Cai Bao, Zhuang Fei Wang, Jing Ma, Nan Ling Zhou and Xiao Hui Hou *

School of Preclinical Medicine, Zunyi Medical University, Guizhou 563099, China
* Correspondence: hxh19801122@163.com

Simple Summary: Highlight: For the first time in this study we have examined the external and internal structures of male and female adults of *Culicoides grisescens* Edwards with scanning electron microscope (SEM) and tissue section techniques. This paper provides visual and descriptive details for the systematic taxonomic study of Ceratopogonidae.

Abstract: The external and internal structures of male and female adults of *Culicoides grisescens* Edwards, were examined with scanning electron microscope (SEM) and tissue section techniques. Specimens were collected from Qilian Mountain National Park in Qinghai Province, China. The ultrastructure and morphology of compound eyes, antenna, maxillary palpus, spermathecae, genitalia and other structural characteristics of both male and female adults of *C. grisescens* are described. Internal structures of the species are described, including histological sections of the digestive, nervous, respiratory, and reproductive systems. This paper provides visual and descriptive details for the systematic taxonomic study of Ceratopogonidae.

Keywords: Biting midge; *Culicoides*; morphology; scanning electron microscope; tissue sectioning

1. Introduction

Culicoides are small biting midges with blood-sucking abilities in the family Ceratopogonidae (Diptera: Culicomorpha). Currently, there are 1347 species in the world and 480 species in China [1,2]. The female adults of many species of biting midges are pests of both people and livestock, causing painful lesions and inducing acute allergic reactions such as common summer eczema in horses [3]. In addition, they can transmit viral and non-viral pathogens, such as Bluetongue virus (BTV), Japanese encephalitis virus (JEV), African horse sickness virus (AHSV), malaria-like parasites *Haemoproteus* [4–6]. Therefore, *Culicoides* are a group of medically important insects. *Culicoides grisescens* is a common species distributed in Europe, Asia, and so on. In China, it is mainly distributed in Xinjiang, Inner Mongolia and other regions with higher elevations [7,8], which all have a large number of farms and well developed animal husbandry. Thus, these areas have an increased risk of midge-borne disease transmission. The identification of *C. grisescens* mainly depends on hand-drawn figures of taxonomic features which often lead to subtle and discriminant features being ignored or being unclear. The cryptic species *C. grisescens* G1 and G2 cannot be distinguished morphologically by light microscopy [9]. Therefore, it is necessary to interpret more comprehensive and subtle morphological features in order to supplement and improve the morphological descriptions. There have been many reports on the hematoxylin - Eosin (HE) staining and paraffin sections of insects [10–14], however, there are fewer reports about the tissue structure of biting midges. In this paper, the morphology and ultrastructure of both adult sexes of *C. grisescens* were observed and described in detail by SEM, describing its characteristic morphology. This will provide an accurate basis for the classification and identification of *Culicoides* populations. At the same time, the inner organizational

 doi:10.20944/preprints202405.1715.v1

structures of *C. grisescens* were systematically studied by using continuous paraffin sectioning, which provides more direct material for studying the development of *Culicoides* and other Ceratopogonidae.

2. Materials and Methods

2.1. Entomological Sampling

Adults *Culicoides grisescens* were collected with traps by the members of the research team in Qilian Mountain National Park in Qinghai Province from July to August 2020. The specimens were stored in 70% ethanol and brought back to the laboratory for identification.

2.2. Sample Preparation

For the SEM study, adults of *C. grisescens* were prepared following the technique of Jiang et al. [15]. *Culicoides grisescens* adult samples were washed with distilled water for 10 minutes, with slight agitation. After cleaning, the samples were dehydrated in 75, 85, and 100% ethanol for 15 minutes in each concentration and stored in 100% ethanol. Drying was carried out in a Leica EM CPD300 automatic critical point dryer. After drying, the specimen was dissected under stereoscope, the dissected parts were attached with double-sided conductive adhesive, and the position recorded. Samples were coated with gold in a Leica EM ACE600. Finally, the ultrastructure was observed by tungsten filament scanning electron microscopy (SU8010), photographed and preserved. The abbreviations used in this paper follow Jiang et al. [16].

For the histological study, the adults were prepared following the technique of Ning et al. and Jiang et al. [16,17]. The wings and legs were removed with fine needles, and the remaining was dipped into the fixative for 24h at room temperature. The following steps were to dehydrate the specimens with different concentrations of ethanol solution (80%, 85%, 90%, 90%, 95%, 95%, 100% and 100%). To prepare the specimens further, they were placed in benzene- and paraffin-embedded at 55°C. Both longitudinal and transverse sections were made (3 μm thick) and then stained with hematoxylin-eosin (HE). Finally, they were soaked in xylene for 10 minutes, mounted on slides with neutral glue, with a coverslip added and dried. Tissues were observed and photographed using a digital system for OLYMPUS BX43 with digital camera DP26.

In the descriptions, specimens were measured for each character and ratios and measurements of the antennae (AR), palpi (PR (III)), wings and costal vein (CR) were obtained following the methods described by Dominiak [18]. Measurements are given for the range, mean and number of specimens examined for each.

3. Results

Culicoides grisescens Edwards, 1939

Figures 1-6

 doi:10.20944/preprints202405.1715.v1

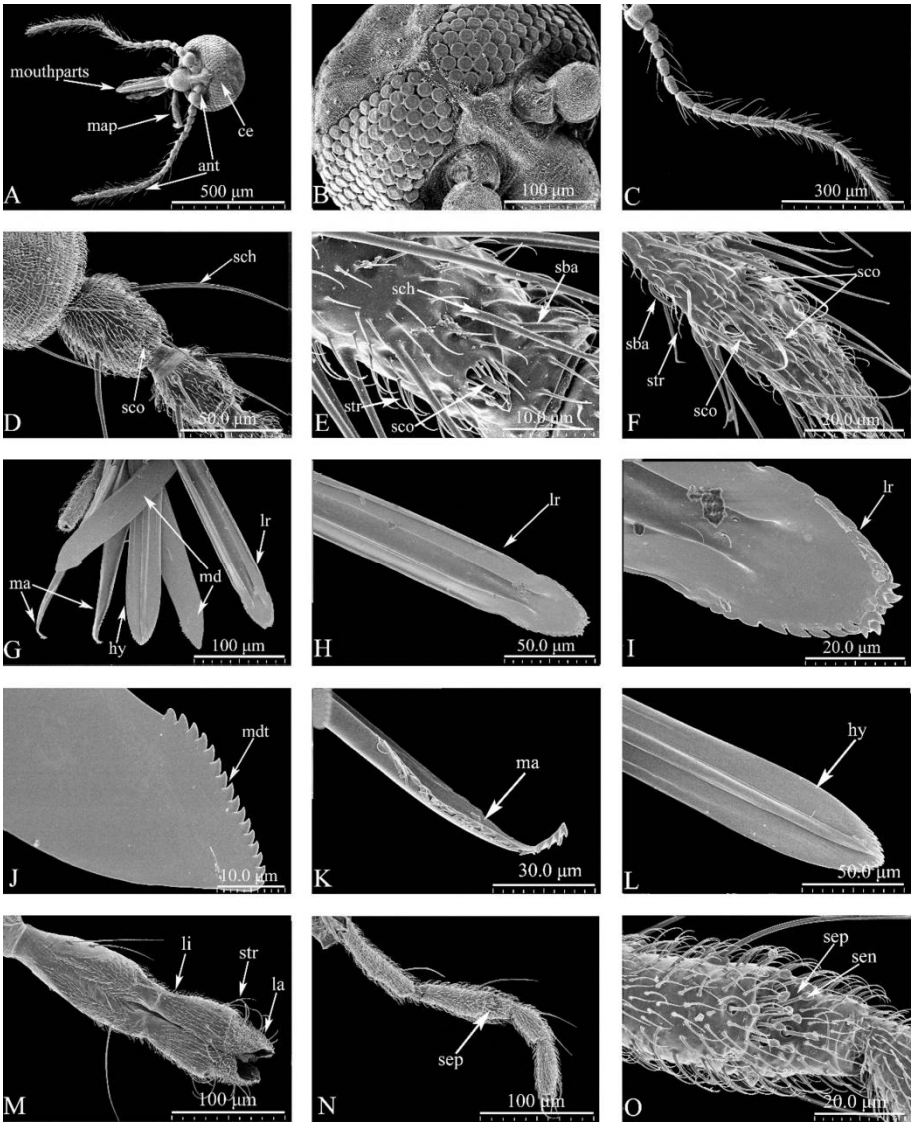

Figure 1. *Culicoides grisescens* adult Head (**A-O**), **(A)** Head, general view; (**B**) frontal sclerite, ommatidium of eye and inter—ocular space, anterior view; (**C**) flagellomeres, anterior view ; (**D-F**) Types of antennal sensill; **(G-M)** Mouthparts, anterior view; **(H-I)** Labrum end part; (**J**)Mandible; **(K)** Maxille; **(L)** Hypopharynx; (**M**)Labium; (**N**)Maxillary palpus; (**O**)Terminal of the 3rd maxillary palpus. ant: antenna; ce: compond eye; hy: hypopharynx; la: Labellum; lr: Labrum; li: labium; ma: maxilIe; map: maxillary palpus; mdt: Teeth of mandible; sba: Sensillum basiconica; sc: Sensillum campanulate; sch: Sensillum chaeticum; sco: Sensillum coeloconica; sen: Sensilla; sep: Sensory pit; str: Sensillum trichodea.

 doi:10.20944/preprints202405.1715.v1

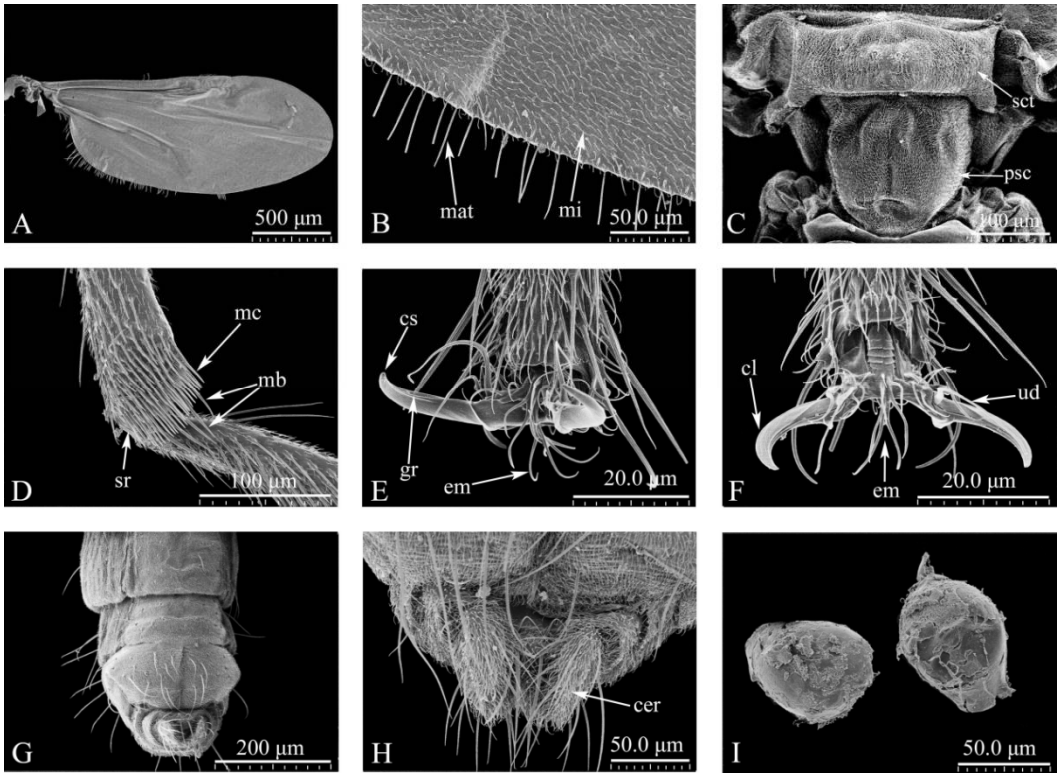

Figure 2. *Culicoides grisescens* adult thorax and abdomen(**A-I**). (**A-B**) Wing surface; **(C)** Scutellum and postscutellum; (**D**)Terminus of hindtibia; **(E)** Claw of Foreleg, Side view; **(F)** Claw of Hindleg, anterior view; **(G)** Genitalia，ventral view; **(H)** Cerci; (**I**) Spermatheca. mat: macrochaeta; mi: microtrichia; sr: spur; sct: scutellum; psc: postscutellum; mc: metatibial comb; mb: metatibial distae bristles; gr: groove; cs: cusp; em: empodium; cl: claw; ud: ungual digitule; cer: cerci.

 doi:10.20944/preprints202405.1715.v1

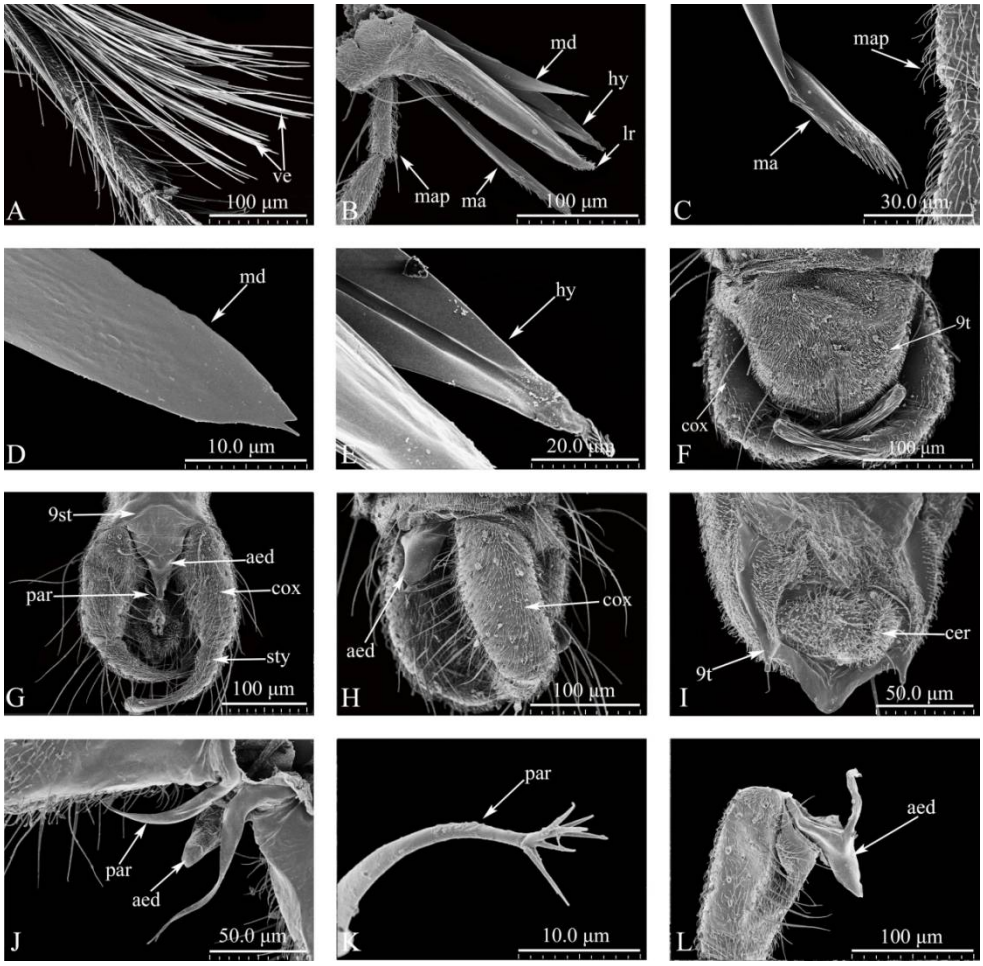

Figure 3. *Culicoides grisescens* adult Male(**A-L**). **(A)** Verticil; **(B)** Mouthparts, anterior view; **(C)** Maxil; **(D)** Mandible; **(E)** Hypopharynx; **(F)** Hypopygium, dorsal view; **(G)** Hypopygium, ventral view; **(H)** Hypopygium, side view; **(I)** The inner hypopygium; **(J)** Verticil; **(K)** Paramere distal portion; **(L)** Aedeagus. aed: Aedeagus; cer: Cerci; Cox: Gonocoxite; la: Labellum; lr: Labrum; mat: Teeth of maxil; mdt: Teeth of mandible; par: paramere; 9t: The 9th tergum; 9st: The 9th stema; ve: verticil; str: Sensillum trichodea; sty: Gonostylus.

 doi:10.20944/preprints202405.1715.v1

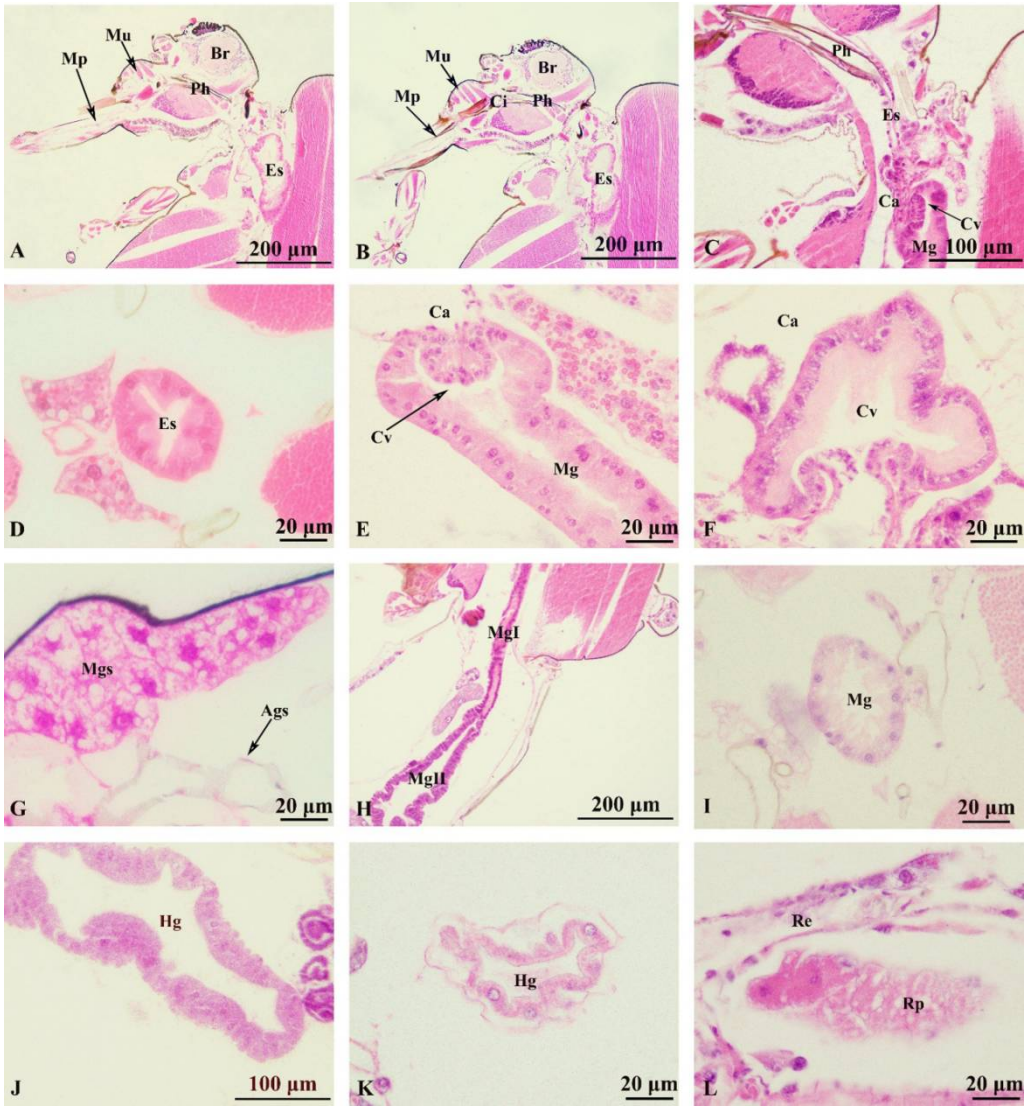

Figure 4. *Culicoides grisescens* Digestive system (**A-L**). **(A)** Longitudinal cutting head; **(B)**Lonitudinal setion of the pharnx; **(C)** Longitulinal setion of the esoprlagus; **(D)** Transverse section of the esophagus; **(E)** Longitulinal setion of the Canlia; **(F)** Transverse section of the Canlia; **(G)** Longitulinal setion of the Salivary glands; **(H)**Lomngitulinal section of the midgut; **(I)** Transverse secion of the midgut; **(J)** Hidgut; **(K)** Malpighian tubules; **(L)** rectum. Ags: Accessory glands; Br: Brain; Ca: cardia; Ci: Cibarium; Cv: cardiacvalve; Es: esophagus; Fg: foregut; Hg: hindgut; Mp: mouthparts; Md: mandibles; Mu: muscle; Mg: midgut; Mgs: Main glands; Mt: Malpighian tubules; Ph: pharynx; Rp: rectal pad; Re: rectum.

 doi:10.20944/preprints202405.1715.v1

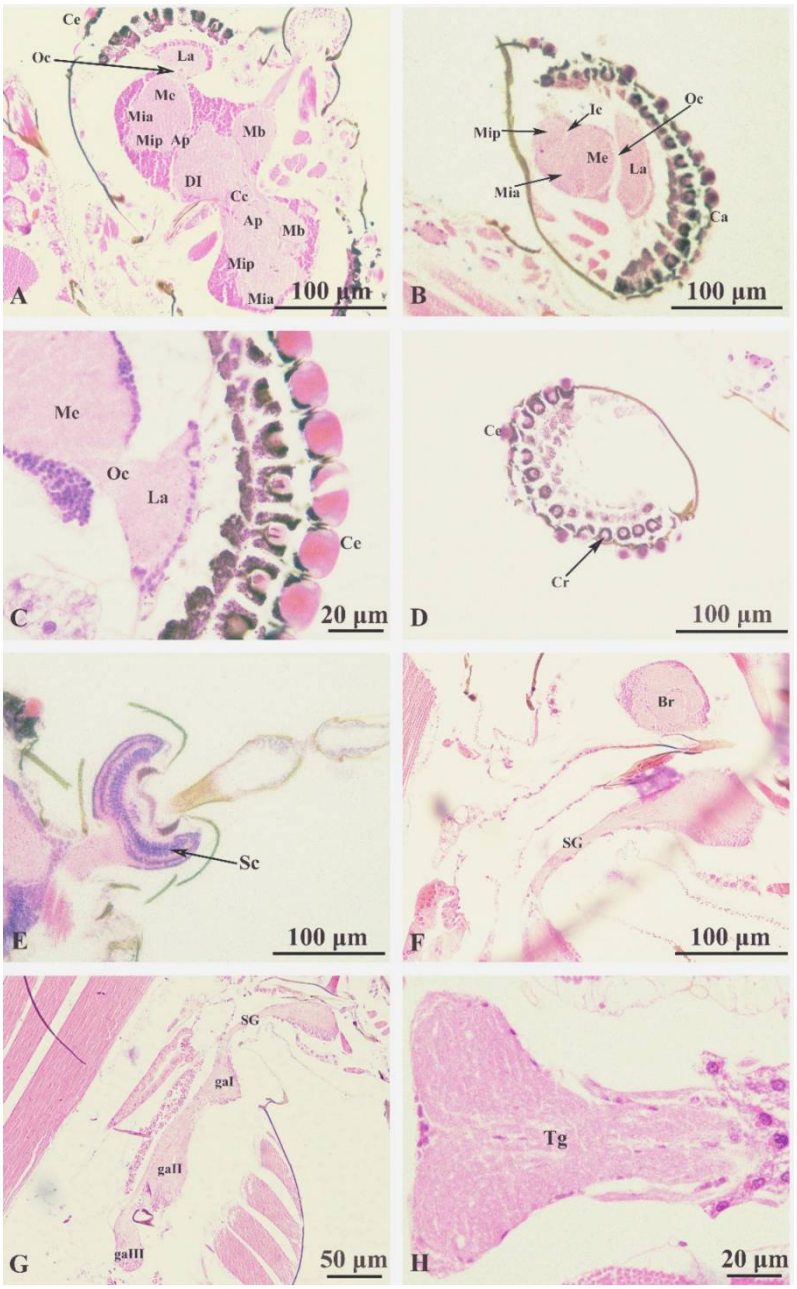

Figure 5. *Culicoides grisescens* Central nervous system (**A-H**). **(A)** Transverse cutting brain; **(B)** Longitudinal cutting brain; **(C)** Optic lobe; **(D)** Compound eye; **(E)** Longitudinal section of scape; **(F)** Subesophageal ganglion; **(G)** Thoracic ganglion, side view; **(H)** Thoracic ganglion, anterior view. Ap: accessory protocerebral lobe; Ce: compound eye; Cc: central complex; Dl: deutocerebrum; ga I: prothoracic ganglion; ga II: mesothoracic ganglion; ga III: posterior thoracic ganglion; Ic: inner chiasma; La: lamina; Me: medulla externa; Mia: anterior lobe of medulla interna; Mip: posterior lobe of medulla interna; Mb: mushroom body; Oc: outer chiasma; Sc: Scapde; SG: suboesophageal ganglion.

 doi:10.20944/preprints202405.1715.v1

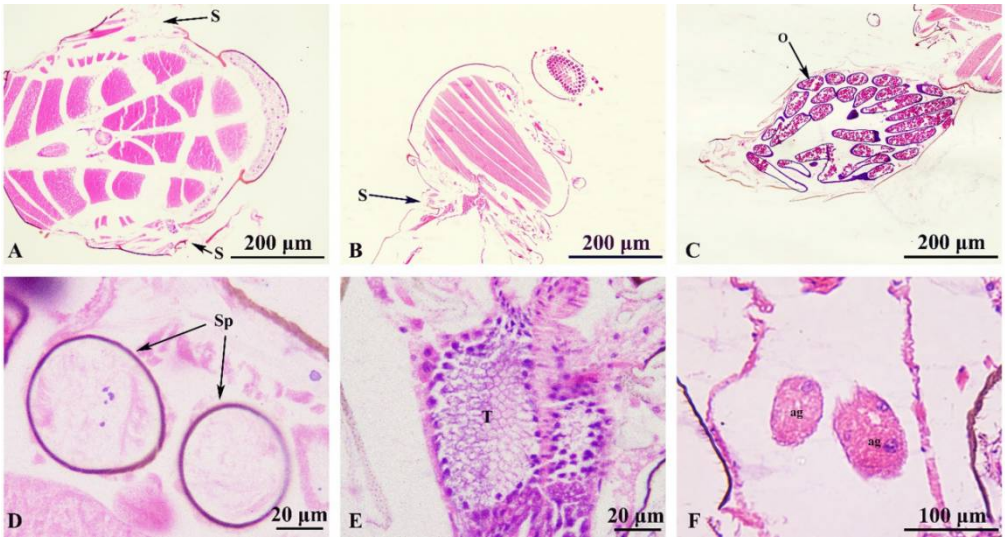

Figure 6. *Culicoides grisescens* Respiratory system and Reproductive system (**A-L**). (**A**) spiracle, anterior view; (**B**) spiracle, side view; (**C**) ovary; (**D**) spermatheca; (**E**) testis; (**F**) accessory glands. ag: accessory gland; O: ovary; Sp: spermatheca; S: spiracle; t: testis.

Material examined. 9 females, 9 males. Maixiu Forest Farm, Zeku County, Huangnan Tibetan Autonomous Prefecture, Qinghai Province, China, 35°27'13.77"N; 101°93'25.62"E, 6.VIII.2020, alt. 2941 m, ZhuangFei Wang leg.

3.1. Redescription of Adults (Figure 1-3).

Female (Figure 1A-O, 2A-I).

Head (Figure 1A-O)**.** General view of head (Figure1A). Dark brown. Eyes contiguous, abutting medially for length of 1.0 ommatidia, without interommatidial spicules, surface bare (Figure 1A, B). Frontal sclerite nearly round, with long, slender ventral projection (Figure 1B). Antennae (Figure 1C) brown, with 13 vasiform shape segments, distal 5 flagellomeres elongate, AR 1.14–1.21 (1.17, n=3). Antennal sensilla distributed on flagellomeres 1-13 increasing in number gradually from base to apex, with many sensillum trichodea and sensilla arranged irregularly; sensilla coeloconica present mainly on flagellomeres 1, 9-13 (Figure 1C-F): two on segments 1 and 12, one in each of 9-11, and three presents on segment 13; sensilla basiconica presents on the distal 5 segments, straight or basal 1/3 slightly curved (Figure 1C-E). Mouthparts well developed, composed of labrum, mandible, maxilla, hypopharynx and labium (Figure 1G): labrum with sunken middle, spike shape apically, distal middle portion flame-shaped (Figure 1H-I). Mandible with narrow and short protuberance in middle, apical portion triangular, with 16 teeth (Figure 1J). Lacinia with two rows of teeth: 16 in the first row and 1 in the second row, apical 3 teeth triangular (Figure 1K). Hypopharynx long, sword-shaped, pointed apically (Figure 1L). Labium with 4 segments, sensilla trichodea, sensilla chaetica and sensilla basiconica present on the 4th segment (Figure 1M). The maxillary palpus with 5 segments, PR 3.34-3.59 (3.47, n=3); 3rd segment slender, slightly swollen apical 1/3; multiple irregular pits with 11-13 hollow capitate sensilla scattered on the surface (Figure 1N-O).

Thorax. Wing length 1.86-2.15 mm (2.03 mm, n=3), width 0.74-0.96 mm (0.85 mm, n=3), CR 0.63-0.65 (0.65, n=3). Wing surface densely covered with microtrichia and macrotrichia, basal cell without macrochaeta (Figure 2A-B). Scutellum trapezoid with four stout and eight fine setae (Figure 2C); postscutellum with surface pubescent (Figure2C). Hind tibia comb with 6 terminal bristles, 1st and 2nd spine longest (Figure 2D). Tarsal claws horn-shaped (Figure 2E-F).

Abdomen. Brown, ventral surface covered with a large number of bristles and spicules (Figure 2G); cercus semicircular (Figure 2I). Two spermathecae, oval, different sizes (71.02 μm×54.82 μm, 68. 62 μm×57.28 μm).

Male (Figure 3A–L).

Head. As in female but for the following sexual dimorphism. Antenna brown, AR 1.02-1.17 (1.07, n=3) (Figure 3A). PR 3.18-3.52 (3.41, n=3). Dorsal surface basal 1/3 of labrum with microtrichia, arranged in a triangle (Figure 3B). Maxille with 20 teeth, some slender and bifurcate, with small teeth

 doi:10.20944/preprints202405.1715.v1

medially (Figure 3C). Mandible with 2 teeth of different sizes (Figure 3D). Hypopharynx long, sword-shaped, with a slender groove medially, apex edge with slender teeth (Figure 3E).

Thorax. Wing length 1.90-2.04 mm (1.99 mm, n=3), width 0.65-0.68 mm (0.67 mm, n=3), CR 0.60-0.63 (0.62, n=3). Wing surface densely covered with microtrichia and macrotrichia, basal cell without macrochaeta.

Abdomen. Genitalia: tergite 9 trapezoidal, gradually narrowing from the base (Figure 3E, I). Medially the 9th sternum with spicules (Figure 3G). Gonocoxite stout, with coarse bristles and fine bristles covering surface (Figure 3G, H). The two cerci separate and on the hypoproct (Figure 3I). Parameres (Figure 3G, J) separate, with median lobe short, thin, lateral lobe curved, slender, gradually narrowing to apex, apex with 5-7 branches, slender finger-like processes (Figure 3J, K). Aedeagus tower-shaped, both sides separated, arch shallow "V" shape, medially concave (Figure 3L).

3.2. Description of Internal Structures of Adults (Figure 4-6).

Digestive system (Figure 4A-4L).

Foregut (Figure 4A-4F). The mouthparts (Figure 4A) with the upper and lower lips, tongue, large and small jaws, are anterior to the digestive tract. Pharynx (Figure 4B) thickening with pharyngeal tube wall; the cibarium protuberance-shaped, connected to the upper and lower tube wall by muscles. Esophagus (Figure 4C, D) is slender and tubular structure, mainly composed of monolayer epithelial cells, connected to the back of the pharynx, the joint at the connecting plane of the head and chest. The cardia (Figure 4C, E, F) is at the end of the foregut and part of the tube wall sunken inward, forming the cardia valve. Salivary glands are located ventrally and anteriorly in the thorax, and each gland was positioned lateral to the foregut and between layers of thoracic muscles (Figure 4G), divided into two glands, left and right, gathered by the salivary gland duct and lead to the saliva pump near the mouthparts. Each gland is divided into two parts, the main gland and the accessory gland. The main gland is grape-like and had an acinar structure surrounded by large secretory cells. The accessory glands processes are at the base of the ducts.

Midgut (Figure 4H-4I). Developed and expanded, extending back from the thorax to the abdomen, located in the posterior part of the cardiac valve and the anterior part of the pyloric node; the intestinal parietal cells are composed of monolayer columnar epithelial cells, neatly arranged with large and round nuclei, mostly located in the middle or base of the cells; midgut with two regions: the first region is long and narrow and the second region is the stomach which is dilated at the enlarged abdominal lumen(Figure 4H).

Hindgut (Figure 4J-4L). The anterior end connects to the midgut and the posterior end connects to the anus; consists of the ileum, colon and rectum (Figure 4J). The malpighian tubules separated from the connection between the hindgut and the midgut (Figure 4K). The differentiation of ileum and colon is not obvious nor easy to distinguish. The anterior part of the rectum swells to form a rectal capsule, with oval glands on the wall called a rectal pad (Figure 4L). The top of the rectal pad goes deep into the rectal cavity and the intima on the surface is thin. The rectal sac narrows gradually and ends at the anus.

Central nervous system (Figure5A-5H).

Brain (Figure 5A). Internal structure complex, located in the head above the pharynx, covered with the cuticle of the head and surrounded by muscle tissue; divided into three parts: protocerebrum, deutocerebrum, and tritocerebrum. The protocerebrum makes up the majority of the brain, with the protocerebral and optic lobes (Figure 5B) connecting the nerves to the compound eye (Figure 5C); divided into the left and right hemispheres. The protocerebral lobe includes a pair of corpus pedunculatum, a central complex and a pair of accessory protocerebral lobes (Figure 5A). This structure is extremely complex and the medullary layer of the protocerebral lobe is formed by bundles of nerve cells and nerve fibers. The optic lobe (Figure 5C) is composed of the anterior lobe of medulla interna, posterior lobe of the medulla interna, medulla externa and lamina, and is on both sides of the protocerebrum, an inner chiasma is formed between the medulla externa and the medulla interna, and the outer chiasma is formed between the medulla externa and the lamina (Figure 5C), the lamina gives out nerve fibers and connects with the compound eye (Figure 5C, D). The deutocerebrum (Figure 5A) located at the medial side of the forebrain, is connected with the protocerebrum in front and the antennal nerve bundle in the back, composed of a pair of dorsal lobes

 doi:10.20944/preprints202405.1715.v1

and a pair of antennal lobes (Figure 5E). The sritocerebrum (Figure 5F) sends out circumoesophageal connected to the subesophageal ganglion around the pharynx.

The ventral nerve cord (Figure 5F-5H). Structurally complex, formed by the fusion of left and right nerve trunks, consists of 1 subesophageal ganglion, 3 thoracic ganglia, and 5 abdominal ganglia. Subesophageal ganglion (Figure 5F) with abundant nerve fiber poles. The three thoracic ganglia (Figure 5G) are located in the anterior, middle and posterior chest respectively, corresponding to the anterior, middle and posterior feet. These send out nerve fibers to the ventral side of the foot and to the back into the base of the wing. Thoracic ganglion (Figure 5H) are highly fused in the thoracic cavity, extremely developed and easy to distinguish. The abdominal ganglion is underdeveloped and the nerve fibers are mainly distributed to the abdominal internal organs.

Respiratory system (Figure 6A-6B)

The tracheal system distributed throughout the body and consists of trachea, bronchi and microtrachea, gradually reduced in diameter and continuously branched, and communicate with the atmosphere through the spiracles. Two pairs of spiracles located in the mesothorax (Figure 6A) and the posterior thorax (Figure 6B). Trachea with expanding airsac, with bubble back sac and air sac.

Reproductive system (Figure 6C-6F)

Female reproductive system (Figure 6C, D) includes the ovary, oviduct, spermatheca, accessory gland. A pair of ovaries, symmetrical, connected with an oviduct, the base of the two oviduct tubes converge and lead to the genital opening (Figure 6C). The ovaries are formed by the ovarian tube, circular, with thin walls; each ovary with several short ovarian tubes that develop into a mature egg cell. The spermatheca is spherical and connected to the spermatheca duct, with the vesicle duct connected to the genital opening (Figure 6D).

Male reproductive system (Figure 6E-F). Including testes, spermaduct, ejaculatory duct and accessory gland. The pair of testes are connected to the ejaculatory duct through the vas deferens, and are symmetrical, containing spermatogonia of different stages, shown with HE staining as a light blue (Figure 6E). A pair of reproductive accessory glands located on both sides of the ejaculatory duct and open to the ejaculatory duct (Figure 6F).

4. Discussion

In this study, the morphological ultrastructure of the male and female adults of *C. grisescens* was observed using scanning electron microscopy (SEM) to obtain improved morphological details of this species and to redescribe its morphological characteristics more accurately. At the same time, the internal structure of the digestive, nervous, respiratory and reproductive systems of *C. grisescens* was analyzed by fixation, sectioning and staining techniques.

Adult ceratopogonidae have a small body length (1~4 mm) and a wide variety of species, including complex groups or species groups composed of related species with similar morphology [19]. It is very important for taxonomists to describe and explain their morphological characteristics comprehensively and accurately. In this study, it was also observed that aedeagus of the male was V-shaped, and the paramere distal portion was bifurcated and had 5-7 branches, which was a slender finger process, which was a supplement to some of the morphological characteristics reported by predecessors.

There is no gastric caecum structure in the digestive tract of *C. grisescens* and the existence and number of this structure are quite different among Diptera [20,21]. Because the main function of the gastric caecum is to increase the surface area of the midgut to assist its digestion and absorption, insects that feed on liquid food do not have this structure. The brain of *C. grisescens* is similar to that of most insects [21]. It can distinguish three typical functional areas: forebrain, midbrain and hindbrain. The thoracic ganglion is highly fused in the chest, indicating that it plays a strong role in controlling movement, and the merging of thoracic ganglia is different in different groups. There are significant differences in the structure of internal reproductive organs between sexes and species. Two round sperm vesicles can be observed in female adults, and the color inside the testis of male adults is different. It is inferred that different colors represent different degrees of sperm maturity. Although the respiratory system of *C. grisescens* is distributed all over the body, only the structure of the valve is observed in this study due to the small limitation of the staining process. The system needs further study.

This study more intuitively and stereoscopically observed the morphological differences between *C. grisescens* female and male mouthparts, such as more mandibular teeth, different arrangement and number of mandibular teeth, narrower and triangular tongue tip in males than females, significant differences in antennal morphology, antennal sensilla types and other morphological characteristics. Because of its obvious sexual dimorphism, synonymous species may appear. Although this study obtained more comprehensive, detailed and vivid structural information on *C. grisescens*, there is a lack of morphological characteristic data similar to its cryptic species. Therefore, in the follow-up work, we will compare the species morphology of different regional distributions of this species and its related species, and obtain relatively stable and reliable morphological characteristic data. This paper is the first to describe the internal structure of this species, mainly including four systems: the digestive system, nervous system, respiratory system, and reproductive system. Due to the limitations of the small size of *C. grisescens* and issue with the research methods, we failed to provide a complete picture of the entire organ system. However, we can observe the basic structure of *C. grisescens* with the slice technique. In conclusion, the insect tissue structure is vital, but has been widely neglected. Further research is warranted as it will illuminate basic aspects of insect physiology, vector-borne disease transmission, and even human disease. This research provides vivid and accurate reference information for the systematic taxonomic study of Ceratopogonidae.

Author Contributions: Conceptualization, X.L. and Y.L.Z.; methodology, X.L. and Y.L.Z.; software, X.L. ; formal analysis, X.L. and Y.L.Z.; investigation, X.L.; resources, S.C.B. and Z.F.W.; data curation, J.M. and N.L.Z.; writing—original draft preparation, X.L. and Y.L.Z.; writing—review and editing, X.L. and Y.Z and X.H.H.; visualization, X.H.H.; supervision, X.H.H.; project administration, X.H.H. All authors have read and agreed to the published version of the manuscript.

Funding: This research was financially supported by the grant from the National Natural Science Foundation of China (31960102).

Data Availability Statement: The data supporting the findings of this study are available from the corresponding author upon reasonable request.

Acknowledgments: We cordially thank Dr. Art Borkent for invaluable advice and comments on the manuscript, and to Dr. Phillip Shults for linguistic and professional assistance during the preparation of this manuscript. We would like to thank the staff who helped us collect *Forcipomyia (Lasiohelea) taiwana*. We are indebted to Lecturer Fengyue Wang for her technical assistance.

Conflicts of Interest: The authors declare no conflict of interest.

References

1. Borkent A, Dominiak P, Díaz F. (2022) An Update and Errata for the Catalog of the Biting Midges of the World (Diptera: Ceratopogonidae). Zootaxa 5120(1): 53-64. https://doi.org/10.11646/zootaxa.5120.1.3.
2. Duan YL, Bellis G, Liu BG, Li L. (2022) Diversity and seasonal abundance of Culicoides (Diptera, Ceratopogonidae) in Shizong County, Yunnan Province, China. Parasite. 2022;29:26. https://doi.org/10.1051/parasite/2022027.
3. van der Rijt R, van den Boom R, Jongema Y, van Oldruitenborgh-Oosterbaan MM. (2008) *Culicoides* species attracted to horses with and without insect hypersensitivity. The Veterinary Journal 178(1): 91-97. https://doi.org/10.1016/j.tvjl.2007.07.005
4. Stewart ME, Roy P. (2015) Structure-based identification of functional residues in the nucleoside-2'-O-methylase domain of Bluetongue virus VP4 capping enzyme. FEBS Open Bio. 5:138-46. https://doi.org/10.1016/j.fob.2015.02.001.
5. Li C, Wang W, Zhang X, Xiao P, Li Z, Wang P, Shi N, Zhou H, Lu H, Gao X, Zhang H, Jin N. (2023) Metavirome Analysis and Identification of Midge-Borne Viruses from Yunnan Province, China, in 2021. Viruses. 15(9):1817. https://doi.org/10.3390/v15091817.
6. Veiga J, Martínez-de la Puente J, Václav R, Figuerola J, Valera F. (2018) *Culicoides paolae* and C. circumscriptus as potential vectors of avian haemosporidians in an arid ecosystem. Parasit Vectors 11(1): 524. https://doi.org/10.1186/s13071-018-3098-8
7. Paslaru AI, Torgerson PR, Veronesi E. (2020) Summer seasonal prevalence of *Culicoides* species from pre-alpine areas in Switzerland. Medical and veterinary entomology 12(15): 1-9. https://doi.org/10.1111/mve.12500

8. Jun Q, Qingling M, Zaichao Z, Kuojun C, Jingsheng Z, Minxing M, Chuangfu C. (2012) A serological survey of Akabane virus infection in cattle and sheep in northwest China. Trop Anim Health Prod. 44(8):1817-20. https://doi.org/10.1007/s11250-012-0168-3.
9. Wenk CE, Kaufmann C, Schaffner F, Mathis A. (2012) Molecular characterization of Swiss Ceratopogonidae (Diptera) and evaluation of real-time PCR assays for the identification of Culicoides biting midges. Vet Parasitol 184(2-4): 258-266. https://doi.org/10.1016/j.vetpar.2011.08.034
10. Liu B, Song YW, Jin L, Wang ZJ, Pu DY, Lin SQ, Zhou C, You HJ, Ma Y, Li JM, Yang L, Sung KL, Zhang YG. (2015) Silk structure and degradation. Colloids Surf B Biointerfaces. 131:122-8. https://doi.org/ 10.1016/j.colsurfb.2015.04.040.
11. Liu W, Wu L, Wang J, Li X, Jin X, Zhu J. (2020) Activity of Vip3Aa1 against Periplaneta Americana. Open Life Sci. 15:133-144. https://doi.org/ 10.1515/biol-2020-0014.
12. Liu X, Li J, Sun Y, Liang X, Zhang R, Zhao X, Zhang M, Zhang J. (2022) A nuclear receptor HR4 is essential for the formation of epidermal cuticle in the migratory locust, Locusta migratoria. Insect Biochem Mol Biol. 143:103740. https://doi.org/10.1016/j.ibmb.2022.103740.
13. Eskin A, Bozdoğan H. (2022) Effects of the copper oxide nanoparticles (CuO NPs) on Galleria mellonella hemocytes. Drug Chem Toxicol. 45(4):1870-1880. https://doi.org/ 10.1080/01480545.2021.1892948.
14. Xun H, Ding KZ, Yang M, Chen HD. (2013) Histological Observation of the Central Nervous System in *Simulium* (*Wilhelmia*) *xingyiense* (Diptera : *Simuliidae*). Chinese Journal of Parasitology and Parasitic Diseases 31(006): 443-447.
15. Abubekerov LA, Mullens BA. (2018) Egg and Larval Morphology of Culicoides sonorensis (Diptera: Ceratopogonidae). J Med Entomol. 55(3):553-560. https://doi.org/ 10.1093/jme/tjx236.
16. Isberg E, Hillbur Y, Ignell R. (2013) Comparative study of antennal and maxillary palp olfactory sensilla of female biting midges (Diptera: Ceratopogonidae: Culicoides) in the context of host preference and phylogeny. J Med Entomol. 50(3):485-92. https://doi.org/ 10.1603/me12235.
17. Ning Y, Li H, Li JH, Zeng WW, Deng JJ, Li YL, Lu X, Jiang XH, Hou XH. (2022) Histological observation of the internal organs and systems of adultCulicoides punctatus (Diptera : Ceratopogonidae). Acta Entomologica Sinica 65 (5):587-594. https://doi.org/10.16380/j.kcxb.2022.05.006
18. Grogan WLJ, Díaz F, Spinelli GR, Ronderos MM. (2019) The Biting Midges of the Caribbean island Curaçao (Diptera: Ceratopogonidae). I. Species in the genus Dasyhelea Kieffer. Zootaxa. 4700(3): zootaxa. 4700.3.1. https://doi.org/10.11646/zootaxa.4700.3.1.
19. Gopurenko D, Bellis GA, Yanase T, Wardhana AH, Thepparat A, Wang J, Cai D, Mitchell A. (2015) Integrative taxonomy to investigate species boundaries within Culicoides (Diptera: Ceratopogonidae): a case study using subgenus Avaritia from Australasia and Eastern Asia. Vet Ital 51(4):345-378. https://doi.org/10.12834/VetIt.515.2463.2
20. Martín-Vega D, Clark B, Ferrer LM, López-Tamayo S, Colwell DD, Hall MJR. (2020) Internal morphological changes during metamorphosis in the sheep nasal bot fly, Oestrus ovis. Med Vet Entomol. 34(4):476-487. https://doi.org/10.1111/mve.12465.
21. Nakayama H. (2012) Complex asymmetric male genitalia of Anevrina Lioy (Diptera: Phoridae). Arthropod Struct Dev. 41(1):35-49. https://doi.org/10.1016/j.asd.2011.08.001.